The Journal of Neuroscience, June 15, 1999, *19*(12):4907–4920

Abnormalities in Neuronal Process Extension, Hippocampal Development, and the Ventricular System of L1 Knockout Mice

Galina P. Demyanenko, Amy Y. Tsai, and Patricia F. Maness

Department of Biochemistry and Biophysics, University of North Carolina School of Medicine, Chapel Hill, North Carolina 27599-7260

In humans, mutations in the L1 cell adhesion molecule are associated with a neurological syndrome termed CRASH, which includes corpus callosum agenesis, mental retardation, adducted thumbs, spasticity, and hydrocephalus. A mouse model with a null mutation in the L1 gene (Cohen et al., 1997) was analyzed for brain abnormalities by Nissl and Golgi staining and immunocytochemistry. In the motor, somatosensory, and visual cortex, many pyramidal neurons in layer V exhibited undulating apical dendrites that did not reach layer I. The hippocampus of L1 mutant mice was smaller than normal, with fewer pyramidal and granule cells. The corpus callosum of L1-minus mice was reduced in size because of the failure of many callosal axons to cross the midline. Enlarged ventricles and septal abnormalities were also features of the mutant mouse brain. Immunoperoxidase staining showed that L1 was abundant in developing neurons at embryonic day 18 (E18) in wild-type cerebral cortex, hippocampus, and corpus callosum and then declined to low levels with maturation. In the E18 cortex, L1 colocalized with microtubule-associated protein 2, a marker of dendrites and somata. These new findings suggest new roles for L1 in the mechanism of cortical dendrite differentiation, as well as in guidance of callosal axons and regulation of hippocampal development. The phenotype of the L1 mutant mouse indicates that it is a potentially valuable model for the human CRASH syndrome.

Key words: neural cell adhesion molecule; L1; axon guidance; cortical dendrites; hippocampus; mental retardation; CRASH

L1 is a transmembrane adhesion molecule with extracellular immunoglobulin and fibronection III-like domains (Schachner, 1991). L1 has been localized to growth cones and processes of postmitotic developing neurons, where it mediates cell adhesion, neurite outgrowth, and axon bundling. Homophilic and heterophilic binding of L1 between cells activates intracellular signal transduction cascades involving tyrosine kinases and phosphatases that are essential for neurite outgrowth in culture (Atashi et al., 1992; Ignelzi et al., 1994; Klinz et al., 1995; Saffell et al., 1997). L1 may also have a role in learning and memory, because antibodies to L1 perturb the induction of long-term potentiation (LTP) in rat hippocampal slices (Lüthi et al., 1994) and prevent passive avoidance learning in the chick (Scholey et al., 1993).

Mutations in the human L1 gene on the X chromosome result in a complex human mental retardation disorder referred to as the CRASH syndrome (Kamiguchi et al., 1998). The manifestations of this disease include corpus callosum hypoplasia, mental retardation, adducted thumbs, spastic paraplegia, and hydrocephalus (Wong et al., 1995). Symptoms vary among affected family members and between families, suggesting the participation of modifier genes. Of the approximately 70 mutations in the human L1 protein, more severe consequences are associated with mutations of the extracellular region, which may disrupt adhesion and signaling, whereas milder symptoms occur with mutations in the cytoplasmic domain, which may alter only signaling (Fransen et al., 1997; Yamasaki et al., 1997).

An animal model would help illuminate the normal function of L1 and facilitate progress in defining the molecular basis of CRASH syndrome. Toward this end, L1 knockout mice have been generated in two laboratories by homologous recombination (Cohen et al., 1997; Dahme et al., 1997). Dr. Philippe Soriano (Fred Hutchinson Cancer Research Center, Seattle, WA) mutated the mouse L1 gene by replacing exons 13 and 14 encoding the sixth immunoglobulin-like domain, resulting in a complete lack of L1 protein or fragments (Cohen et al., 1997). These L1-minus mice make errors in corticospinal axon guidance (Cohen et al., 1997), have dilated brain ventricles, and perform poorly in a spatial learning paradigm (Fransen et al., 1998). A different L1 knockout strain, produced in the Schachner laboratory by insertional mutagenesis of exon 8 (Dahme et al., 1997), displays a reduced size of the corticospinal tract and decreased axonal association with nonmyelinating Schwann cells. Ventricular enlargement in this L1 knockout strain is highly dependent on the genetic background of the mice, suggesting that modifier genes strongly influence the L1 phenotype (Dahme et al., 1997). Corpus callosum agenesis, which is common in human patients with L1 mutations, has not yet been reported in L1 knockout mice.

Here we report new findings of abnormal morphogenesis of cortical dendrites and developmental defects in the hippocampus and corpus callosum of an L1 knockout mice strain (Cohen et al., 1997). These new findings suggest a biological role for L1 in the mechanism of cortical dendrite differentiation, as well as in hippocampal development and callosal axon guidance, and underscore the potential for this animal model in the study of the CRASH syndrome.

Received Nov. 30, 1998; revised March 8, 1999; accepted March 30, 1999.

This work was supported by National Institutes of Health Grants HD35170 and NS26620. We thank Dr. Philippe Soriano for the L1 mutant mice, Dr. Andrew Furley for advice on PCR genotyping, Dr. John Hemperly for L1 antibodies, and Dr. Jean Lauder, Dr. Patrick Willems, and Dr. Anthony LaMantia for helpful suggestions.

Correspondence should be addressed to Patricia F. Maness, Department of Biochemistry and Biophysics, CB 7260, University of North Carolina School of Medicine, Chapel Hill, NC 27599-7260.

MATERIALS AND METHODS

Production and genotyping of L1 mutant mice

Heterozygous L1 (±) female mice on a 129/SvJae congenic background were obtained from Dr. Philippe Soriano (Fred Hutchinson Cancer Research Center), who produced the mutant mice by homologous recombination in embryonic stem cells (AB-1) (Cohen et al., 1997). The mouse L1 gene was mutated by replacing exons encoding the sixth immunoglobulin-like domain with a *neo* cassette. Because the L1 gene is on the X chromosome, the L1 heterozygous females were bred with wild-type 129/SvJae male mice to generate hemizygous (−/Y) L1-minus males, heterozygous females, and wild-type mice. Wild-type male control animals were produced from the same breeding pairs as L1-minus males. RNA isolated from the brain of these L1 mutant mice contained no L1 transcripts detectable by RT-PCR (Fransen et al., 1998). Neither the full-length 200 kDa L1 protein nor the shorter fragments were detected by immunoblotting (Cohen et al., 1997). In addition, we observed no L1 immunoperoxidase staining in the brain or retina of L1-minus males. This lack of L1 detection indicates that this L1 knockout mouse strain is most likely a null mutation.

Genotypes of mutant mice were determined by PCR analysis. Genomic DNA was isolated from tail segments of mice as described (Morse et al., 1998), except that 1 mM Na-EDTA was used in the lysis buffer. The L1 mutant allele was detected by a 278 base pair DNA fragment generated by PCR using a 5′ primer that anneals to the *neo* sequence (5′-TGG AGA GGC TAT TCG GCT ATG AC) and a 3′ primer in the L1 sequence (5′-AGC AAG GTG AGA TGA CAG GAG ATC). A wild-type L1 allele was detected by a 400 base pair PCR product generated using the 5′ primer (5′-AAG GTG CAA GGG TGA CAT TCA) and the 3′ primer (5′-ACC TCA TCC AGT TCA GTG CTG G). A region of the Y chromosome was amplified using the primers 5′-TGT TCA GCC CTA CAG CCA CAT G and 5′-CCA CTC CTC TGT GAC ACT TTA GCC. Template DNA (0.15 μg) and primers (0.2 μM) were added to a 100 μl reaction containing 1.5 mM $MgCl_2$, 0.2 mM dNTPs, 0.2 μM each primer, and 0.125 U/μl *Taq* polymerase. Amplification was for 30 cycles of 55°C for 0.5 min, 72°C for 1.5 min, and 94°C for 0.5 min.

Histology and immunostaining

Nissl staining and Golgi impregnation. Postnatal day 0 (day of birth) and adult (138–196 d of age) mice were anesthetized with 20% urethane (0.1 ml/10 gm) and perfused transcardially with 1% paraformaldehyde, 1.25% glutaraldehyde, 0.13 M Na-phosphate buffer, pH 7.4. Brains were removed and stored at 4°C overnight in the same fixative, followed by storage for 2–3 d at 4°C in 30% sucrose, 0.13 M phosphate buffer. Frozen serial sections were cut at 40 μm in the indicated orientation on a Minotome Plus microtome (Triangle Biomedical Sciences) and collected in 30% sucrose, 0.13 M phosphate buffer, pH 7.4. The level of the section was indicated by Bregma distances from the interaural line as defined in Franklin and Paxinos (1997). Sections were processed for Nissl (Paxinos and Watson, 1986). For Golgi impregnation, celloidine-embedded brains were cut at 140 μm in frontal orientation, and sections were dehydrated in a graded ethanol series followed by xylene, then embedded in Canada balsam. Golgi staining was performed as described (Marin-Padilla, 1987).

Immunoperoxidase staining. Mouse embryos (8 or 18 d gestational age) were killed by decapitation and fixed without perfusion in 4% paraformaldehyde in Na-phosphate buffer, pH 7.4. Postnatal day 33 and adult mice were anesthetized with 20% urethane and perfused transcardially with 4% paraformaldehyde, 0.13 M Na-phosphate buffer, pH 7.4. Brains were stored at 4°C overnight in fixative, followed by 4°C in 30% sucrose, 0.13 M Na-phosphate buffer for 2–3 d. Frozen sections were cut at 9 μm (embryos) or 24 μm (postnatal and adult), blocked in 10% normal goat serum, 2% BSA, washed in PBS, then incubated with primary antibodies at 4°C overnight. Sections were washed in PBS and incubated with secondary antibodies for 2 hr at room temperature. The remaining steps of immunocytochemistry were performed by the avidin–biotinylated peroxidase method using a Vectastain Kit according to manufacturer's protocol (Vector Laboratories, Burlingame, CA) as described previously (Sorge et al., 1984). Sections were counterstained with toluidine blue and photographed under bright-field illumination. The following primary antibodies were used for immunostaining: rabbit polyclonal antibody 6096 directed against human brain L1 protein [the gift of John Hemperly, Becton Dickinson Technologies, Mountain View, CA (1.4 μg/ml final concentration)], rat monoclonal antibody 324 against L1 (Boehringer Mannheim, Indianapolis, IN), rabbit polyclonal antibody against glial fibrillary acid protein (GFAP; Dako, Carpinteria, CA), and mouse monoclonal antibody SML-99 against myelin basic protein (Sternberger Monoclonal).

Double immunofluorescence staining and confocal microscopy. Wild-type mouse brains [embryonic day 18 (E18)] were fixed as described above, and frozen sections were cut at 10 μm. Sections were permeablized with 0.5% Triton X-100 for 5 min, then washed in PBS, 0.1% bovine serum albumin (PBS-BSA). Sections were incubated with a mouse monoclonal antibody against microtubule-associated protein 2 (MAP2), a neuron-specific marker localizing to dendrites and cell bodies (Amersham, Arlington Heights, IL; 1/1000; specific for MAP2a and MAP2b), together with rabbit polyclonal antibody 6096 against L1 (1.4 μg/ml). Normal mouse IgG and normal rabbit IgG were used at the same concentrations as controls. After they were washed in PBS-BSA, sections were incubated with rhodamine-conjugated goat anti-mouse IgG (1/200) and fluorescein-conjugated goat anti-rabbit IgG (1/100) for 1 hr. Sections were washed in PBS-BSA and mounted in Vectashield for microscopy. Confocal and differential interference contrast microscopy was performed at the University of North Carolina Microscopy Services Laboratory (Dr. Robert Bagnell, Director). Color overlay images were made using Adobe Photoshop and The Image Processing Tool Kit (version 2.5; John and Chris Russ; http://members.aol.com/ImagProcTK).

Measurements of cerebral cortex, commissures, and hippocampus

Cerebral cortex. Serial 40 μm frontal sections (17–76 sections/mouse) spanning the indicated cortical region were subjected to Nissl staining. The width of the cerebral cortical area from the pial surface to white matter was measured at five to nine sites in each section using a measuring reticle in the eyepiece of a Zeiss research microscope, and results were averaged. The mean width of the cortical region per mouse and mean width of the cortical region in the population of mice were calculated with SEs.

Corpus callosum and other commissures. Serial frontal sections spanning the entire corpus callosum of wild-type and L1-minus mice were subjected to Nissl staining and examined microscopically for the presence of the corpus callosum. The rostrocaudal length of the corpus callosum was calculated as the product of the number of sections on which the corpus callosum was present multiplied by the thickness of the coronal sections (40 μm). The dorsoventral thickness (width) of the corpus callosum was directly measured in the same series of Nissl-stained frontal sections spanning the corpus callosum. The dorsal and ventral borders of the corpus callosum were clearly seen by Nissl staining.

The dorsoventral thickness of anterior and posterior commissures was measured in the same Nissl-stained serial frontal sections using a measuring reticle mounted in the microscope eyepiece. The mediolateral dimension was measured for the anterior commissure in a similar manner. The rostrocaudal length of the anterior and posterior commissures was calculated as the product of the number of sections on which these structures were present multiplied by the thickness of the sections (40 μm). Individual and population means and SEs were calculated. Mutant and control groups were compared for significant differences in means using one- or two-tailed versions of the *t* test.

Hippocampus. The number of neurons and glia in the pyramidal and granular layers was determined from cell counts in frontal sections as described by Braitenburg and Schüz (1983). Serial frontal sections spanning the hippocampus (approximately 50 sections per mouse) were subjected to Nissl staining. First, the number of pyramidal, granule, or glial cells in a test unit of volume ($100 \times 250 \times 40\ \mu m^3$) within the pyramidal or granular layer was determined for each section from cell counts using a micrometer inserted in the eyepiece of the microscope. The mean cell number in the test volume for all sections was then calculated. Neurons were distinguished from glia by morphological criteria and Nissl staining pattern. The total number (N) of neurons or glia in the pyramidal or granular layer (one hemisphere) was determined from the mean number of cells (n) per test volume (t) multiplied by the volume (V) of the layer: $n = (n/t)\ V$.

To determine the volume (V) of the pyramidal or granular layer, serial frontal sections (approximately 50 per mouse) were analyzed after Nissl staining. "Test widths" of a given layer were measured using the measuring reticle at five to nine sites within each section, and results were averaged to produce a mean width (in micrometers) in each section. The mediotemporal length (in micrometers) of the layer was determined in each section by summing many short straight lengths across the curved layer. Next, a test volume (v) of the layer in each section was calculated as a product [v = mean width of layer × mean length of layer × section

thickness (40 μm)]. The total volume of the layer (V) was calculated by summing the test volumes of each section [$V = v_1 + v_2 + v_3 + \ldots$].

These estimates were in error to the extent that the sum of linear measurements used to evaluate the length of the layer in a section deviated from the curvilinear dimension, and to the extent that the test volume of the layers in each section deviated from that of a rectangular prism. Additionally, the section thickness was not measured but was assumed to be 40 μm based on the microtome setting. Any cells displaced from the cell body layers were not included in the cell counts. Despite these limitations the same criteria were applied to mutant and wild-type animals, so that differences in means were directly comparable.

Quantitation of degree of linearity of apical dendrites of pyramidal neurons

Apical dendrites of layer V pyramidal neurons in the visual cortex of three L1-minus and three wild-type adult mice were analyzed in frontal sections after Golgi impregnation. Apical dendrites were traced on the computer screen, and their curvilinear lengths were measured by computer-assisted image analysis using the program Scion Image 1.62a at the University of North Carolina Microscopy Services Laboratory. A linearity index (L) was defined as the curvilinear distance (in micrometers) of the region of the apical dendrite measured, divided by the linear distance between the ends of the region of dendrite measured. More than 50 apical dendrites were measured for each genotype. Mean linearity indices and SEs were computed, and differences were analyzed by a two-tailed t test.

Terminal deoxynucleotidyl transferase (TdT)-mediated deoxyuridine triphosphate (dUTP)-biotin nick end-labeling assay

Brains of mice at postnatal days 0 and 10 were subjected to cryostat sectioning at 10 μm in the frontal plane. To detect apoptotic DNA fragmentation, a TUNEL [terminal deoxynucleotidyl transferase (TdT)-mediated deoxyuridine triphosphate (dUTP)-biotin nick end labeling] kit was used (ApoTag, Intergen, Purchase, NY). In brief, after blocking of endogenous peroxidase, sections were incubated at 37°C for 1 hr in reaction mixture containing terminal transferase, digoxigenin-dUTP, and dATP or PBS in controls. Sections were then incubated with peroxidase-conjugated anti-digoxigenin antibody for 30 min at room temperature. After rinsing in PBS, DNA strand breakage was visualized using diaminobenzidine. Nonapoptotic nuclei were counterstained with hematoxylin. The following levels of the brain were analyzed: (1) the rostral dentate gyrus where the suprapyramidal blade is not connected to the infrapyramidal blade, (2) the middle dentate gyrus where the suprapyramidal and infrapyramidal blades are joined and the dentate gyrus is oriented horizontally, (3) the temporal dentate gyrus where the suprapyramidal and infrapyramidal blades are joined and the dentate gyrus is oriented obliquely, (4) the pyramidal layer of the hippocampus, and (5) the septum. Images were captured with a Nikon FXA microscope and Optronics TEC-470 CCD Video Camera System using an Apple Macintosh 840AV computer with a Scion LG-3 capture card. TUNEL-positive cells were scored within areas measured from computer images using the public domain NIH Image software. The accuracy of the cell counting method was established by comparison of counts of TUNEL-labeled cells per unit area made in the microscope and from computer images. For each level of the dentate gyrus, four frontal sections were scored for TUNEL-positive cells, and the area of the region scored was measured from computer images. For the pyramidal layer and septum, 12 sections each were analyzed similarly. For each section the number of TUNEL-positive cells per 10^6 μm^2 was determined, and results were averaged for each mouse. The mean number of TUNEL-positive cells per 10^6 μm^2 was calculated for each population of mice examined, and SEs were determined. Means were compared for statistical differences by a two-tailed t test at $p < 0.05$.

RESULTS

Enlarged ventricles and septal defects in L1 mutant mice

Serial frontal sections of the brains of adult L1-minus male mice were compared histologically with those of wild-type adult males by Nissl staining (Fig. 1*A,B*). In all mutant mice (six of six) there was an obvious enlargement in the ventricular system of the brain, with some variation among individuals in the region of dilation. Significant dilation was observed in the lateral ventricles of five of six mutant mice from approximately Bregma +1.78 mm (Franklin and Paxinos, 1997) to caudal parts of the brain (Fig. 1*B*, *LV*). There was little individual variation in the Bregma coordinates of the lateral ventricles among the L1-minus mice. The dorsal third ventricle was dilated in five of six L1-minus mice and was moved in the rostral direction (from Bregma +1.34 mm to +1.18 mm). The ventral region of the third ventricle was enlarged in only one mouse not showing a dilation of the dorsal third ventricle. The aqueduct (Sylvius) connecting the third and fourth ventricles was dilated in all L1-minus mice. The fourth ventricle was slightly enlarged in two of six mutant mice (data not shown). In contrast to humans with CRASH symptoms, massive hydrocephalus was not apparent in any of the mutant mice. Another prominent malformation found in the L1-minus brain occurred in the septum. Septal nuclei are the source of cholinergic and GABAergic afferents that modulate hippocampal interneuron and pyramidal cell activity (Freund and Antal, 1988), and they provide a minor input to dentate granule cells (Mosko et al., 1973). In L1-minus mice the septal nuclei appeared smaller and split at the medial line seen at the level of the enlarged dorsal third ventricle (Fig. 1*Ba,Bb*). This midline separation corresponded only to sites of enlargement of the dorsal third ventricle and may be a consequence of its dilation.

The cerebral hemispheres of L1 mutant mice were displaced laterally in the middle region of the brain enlarging the longitudinal fissure on the ventral surface (Fig. 1*Bd,Be*). The hippocampus of L1 mutant mice was observed to be displaced laterally from the midline [Fig. 1, compare *Ad,Ae* (wild type), *Bd,Be* (L1-minus)]. The hippocampus and superior colliculus were shifted to a slightly more rostral position (Fig. 1*Bc*), apparently by a small distortion of the ventral relative to the dorsal region of the mutant brain. The superior colliculus was distinquished from the thalamus by labeling with the lipophilic dye DiI and appeared enlarged. A DiI crystal placed into the presumptive superior colliculus of the fixed brain of an L1-minus mouse produced labeling of axons of the optic tract and of some axon bundles that reached the lateral geniculate body (data not shown). The L1-minus brain appeared anatomically normal in regard to the thalamus, basal ganglia, and internal capsule. The cerebellum was generally normal and all cell layers were present, but slight hypoplasticity was noted in the vermis, in agreement with the study of Fransen et al. (1998). The retina exhibited normal cytoarchitecture by hematoxylin and eosin staining, with all nuclear and plexiform layers in the proper orientation and of generally normal size (data not shown). However, one or both eyes of the mutant mice were often partially closed and had a discharge that worsened with maturation of the mice. It is not known whether the L1 mutant mice had visual defects.

Dysgenesis of the corpus callosum

Examination of the corpus callosum in serial Nissl-stained sections showed that in six of six L1-minus mice the corpus callosum failed to form properly. Although there was some variation in the extent of the pathology, in most (five of six) of the L1-minus mice the corpus callosum formed only a small commissure in the medial region of the brain (Bregma 0.38 mm) but was not present in the more caudal (Fig. 1*B*) or rostral sections (data not shown). In one mouse no corpus callosum formed at all. Measurement of the corpus callosum of six L1-minus and nine wild-type mice revealed that the mean rostrocaudal length of the callosum of mutant mice was reduced by 81% compared with wild-type mice

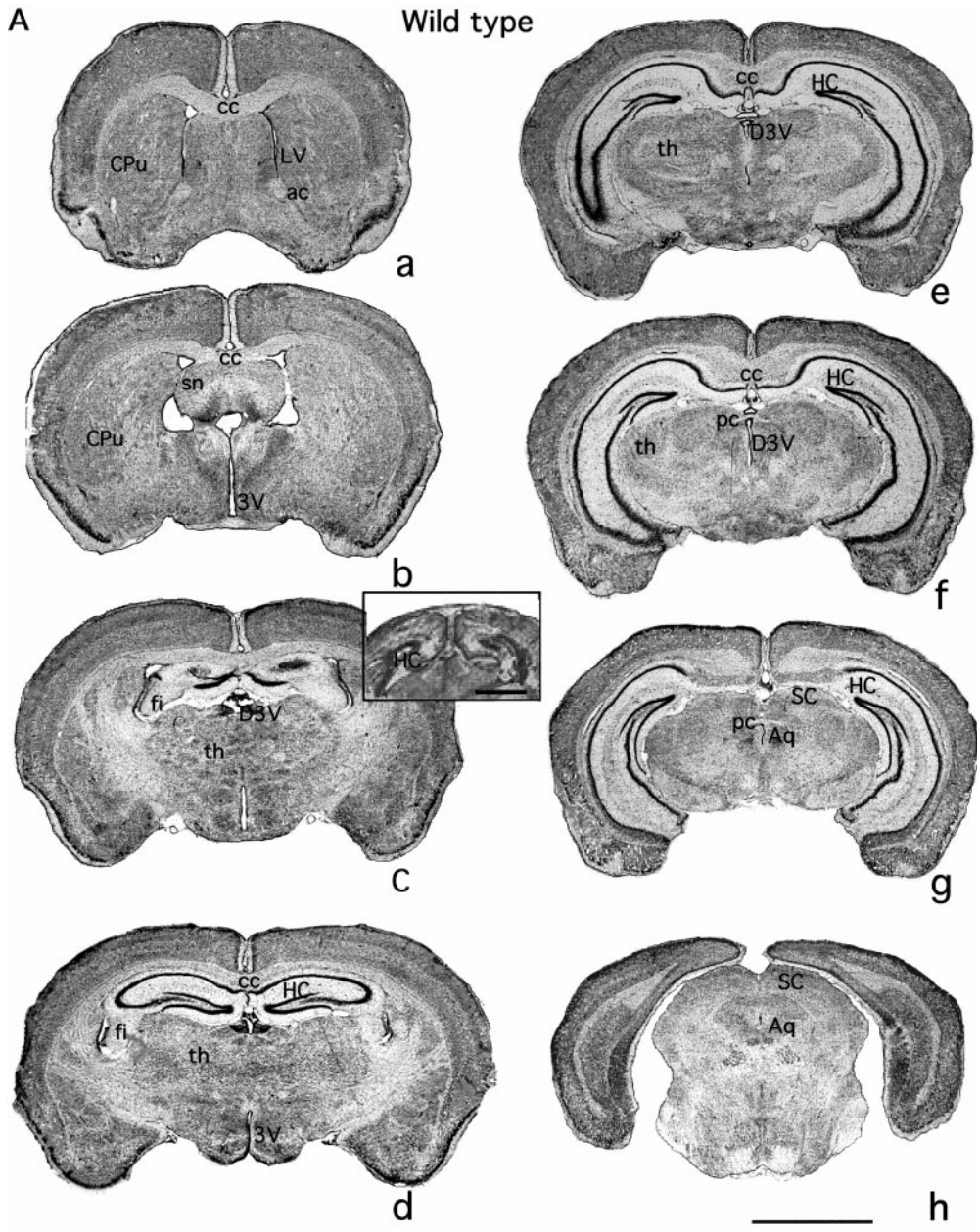

Figure 1. Nissl-stained sections of brains of wild-type (*A*) and L1-minus (*B*) mice showing anatomical differences in the ventricles, corpus callosum, septum, and hippocampus. Serial frontal sections in rostral to caudal direction (*a–h*) were stained by the Nissl technique. Wild-type and mutation sections (*a–h*; Bregma 0.50–4.16 mm, wild type) are from corresponding anatomical levels. Scale bar, 2500 μm. *Insert* in *C* shows corresponding anatomical levels from postnatal day 0 mice. No corpus callosum is apparent at this stage in wild-type (Fig. 1*A*, *insert* in *c*) or L1-minus mice (Fig. 1*B*, *insert* in *c*). Scale bar, 1000 μm. *ac*, Anterior commissure; *Aq*, aqueduct of Sylvius; *cc*, corpus callosum; *CPu*, caudate putamen; *D3V*, dorsal third ventricle; *f*, fornix; *fi*, fimbria; *LV*, lateral ventricle; *sn*, septal nuclei; *3V*, third ventricle; *th*, thalamus; *HC*, hippocampus; *SC*, superior colliculus; *Pb*, Probst bundle; *pc*, posterior commissure. (*Figure continues*.)

(Table 1). The mean dorsoventral thickness of the L1-minus corpus callosum was approximately half that of wild type (Table 1). The differences in mean values were statistically significant by the two-tailed *t* test ($p \leq 0.008$). When the single mouse with no corpus callosum was omitted from the analysis, the mean length (487 μm ± 137) and dorsoventral thickness (132 μm ± 21) of the L1-minus corpus callosum were still significantly different from the wild-type dimensions. The mean body weights of mutant and wild-type mice were similar (Table 1). In most of the mutant mice, callosal axons appeared to grow from the periphery of the brain toward the midline, but instead of crossing the midline they formed large ipsilateral whorls of callosal axons known as Probst bundles (Fig. 1*Ba–Bc*, *Pb*). These bundles stained positively for myelin basic proteins and glial fibrillary acid protein (see Fig. 4*K,L*). The presence of Probst bundles suggested that the initial cortical growth of at least some callosal axons that occurs on radial glia (Norris and Kalil, 1991) did not rely critically on L1.

It is apparent that it would be impossible for axons to cross in the caudal regions where the two cortices are not joined (Fig. 1, compare *Ad, Bd*). Thus the failure of callosal axons in this region to cross the midline may be the result of a physical barrier arising from L1-associated defects in closing of the longitudinal fissure

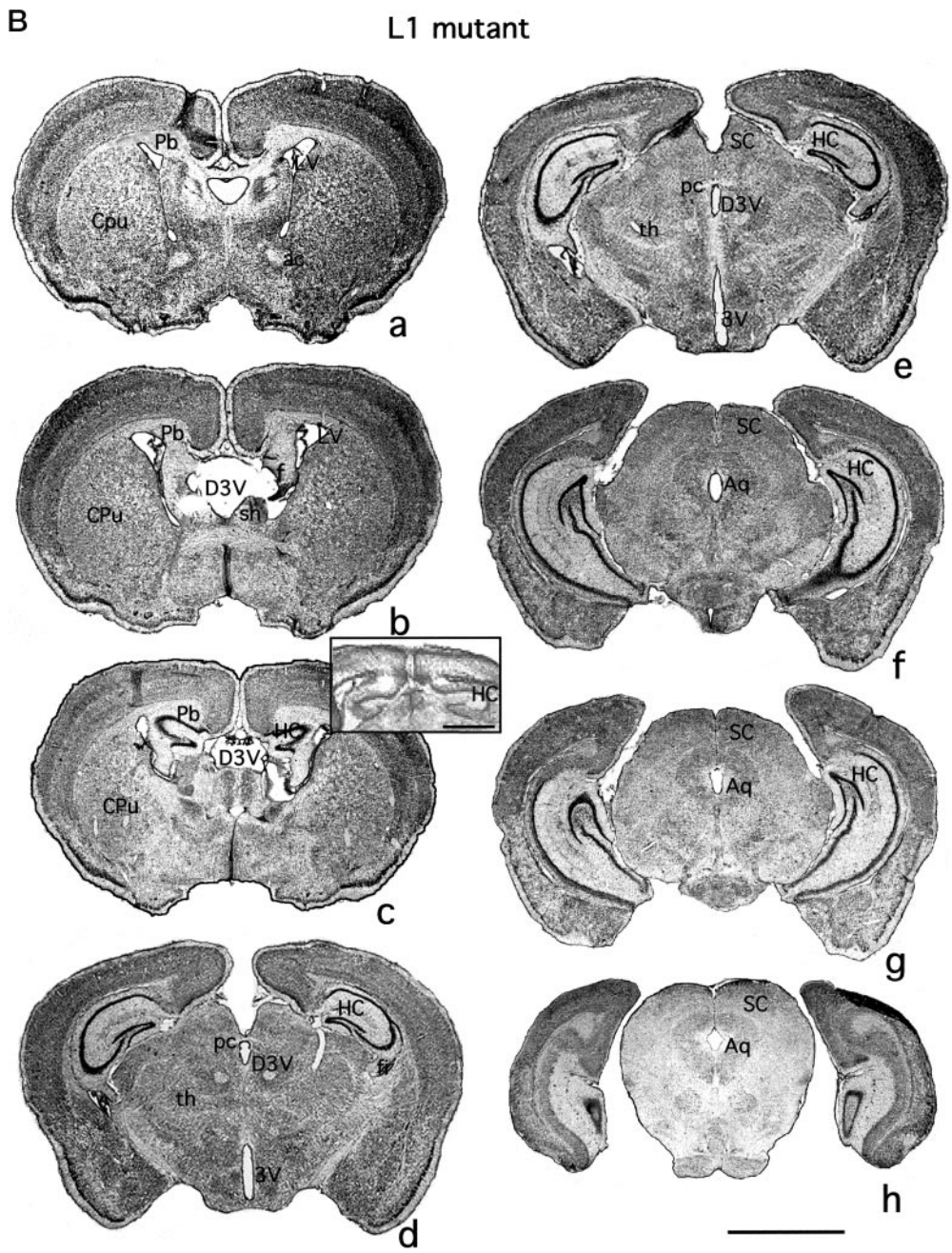

Figure 1 continued.

and perhaps the enlargement of the superior colliculus. However, defective axon crossing near the rostral end of the hippocampus (Fig. 1*Ba–Bc*) was not likely caused by a physical barrier, because the two hemispheres of L1-minus mice in this region were joined in adults. Furthermore, this region did not appear to be separated at earlier stages of development, because at postnatal day 0, when there is no significant axon crossing in this region in wild-type mice (Fig. 1*A*, *insert* in *c*), the cortices of L1 mutant mice were joined (Fig. 1*B*, *insert* in *c*).

Callosal agenesis, commonly present in patients with CRASH syndrome, was not observed by Cohen et al. (1997). They reported the presence of corpus callosal fibers crossing the midline in L1-minus mice but did not make comparative measurements. Corpus callosal dysgenesis in mice is a multigenic defect; thus differences in phenotype can be caused by the contribution of genetic modifiers. The mice studied here were maintained on the original 129/SvJae background, whereas those of Cohen et al. (1997) were crossed onto a different substrain (129/SvEv) (Dr. A. Furley, personal communication) that differs at other loci (Simpson et al., 1997). Other major commissural pathways were not obviously affected by the L1 mutation. The anterior and posterior commissures of L1-minus mice were not significantly smaller than wild-type controls in the rostrocaudal or dorsoventral dimensions (Table 1; Fig. 1, *ac, pc*). There was also no difference in the mean mediolateral dimension of the anterior commissure of L1-minus mice (324 μm $\pm$ 14) compared with wild-type mice (301 μm $\pm$ 16). The anterior commissure did appear to be moved ventrally relative to its normal location, possibly a result of the increased

Table 1. Agenesis of the corpus callosum in L1-minus mice

	Length (μm ± SEM) (rostrocaudal)	Thickness (μm ± SEM) (dorsoventral)	Mean body weight (gm ± SEM)
Corpus callosum (*n*)			
Wild type (9)	2080 ± 369	245 ± 17	23.1 ± 1.1
L1-minus (6)	403 ± 138*	110 ± 28*	23.0 ± 1.8
Anterior commissure (*n*)			
Wild type (5)	1276 ± 64	296 ± 6	23.7 ± 0.8
L1-minus (5)	1220 ± 111	262 ± 22	22.6 ± 2.1
Posterior commissure (*n*)			
Wild type (5)	474 ± 44	111 ± 17	23.7 ± 0.8
L1-minus (3)	653 ± 35	87 ± 3	26.0 ± 0.6

n, Number of mice, frontal sections.

*Significant difference in two-tailed *t* test ($p \leq 0.008$).

size of the lateral ventricles. We do not know whether the hippocampal commissure formed normally in L1-minus mice because axons comprising this small commissure could not be distinquished by Nissl staining from callosal axons with which they intermingle (Livy and Wahlsten, 1997). An intact optic nerve and chiasm were present in adult L1 mutant mice and appeared normal (data not shown). DiI-labeling studies in the same strain of L1 knockout mice showed that retinal axons cross the chiasm (Cohen et al., 1997).

Reduced number of hippocampal cells in L1 mutant mice

Quantitative estimates applied to three L1-minus and four wild-type adult mice revealed ~30% fewer pyramidal and granule neurons throughout the pyramidal and granular layers of the L1-minus hippocampus (Table 2). The mean volumes of the pyramidal and granular layers of the mutant hippocampus were correspondingly decreased (Table 2). The values for wild-type mice were in accord with values reported by others for the number of pyramidal cells (3×10^5) and granule cells (7×10^5) and the volume of the pyramidal layer (0.91 mm^3) in a hemisphere of the adult mouse hippocampus (West and Anderson, 1980; Braitenberg and Schüz, 1983).

The mean number of glia in the pyramidal and granular layers of L1 mutant mice was reduced by 37 and 27%, respectively; however, only the mean number of glia in the pyramidal layer was significantly different from wild type by the *t* test (Table 2). The observed decrease in hippocampal cell number within the pyramidal and granular layers was not a mere reflection of the size of the mice, because the mean body weight of the particular L1-minus mice analyzed was the same or slightly larger than that of the wild-type controls (Table 2). Mean body weight was not significantly different in a larger sample of adult L1-minus males (23.0 gm ± 1.8; $n = 6$) and wild-type 129/SvJae mice (23.4 gm ± 0.8; $n = 10$) of the same age (138–206 d). Although L1-minus juveniles are smaller than normal (Cohen et al., 1997; Dahme et al., 1997), in adulthood they reach ≥80% of the size of normal littermates (Cohen et al., 1997).

The majority (85%) of granule cells of the dentate gyrus are generated in the first 2 postnatal weeks from the secondary proliferative zone in the hilus (Gould et al., 1991). At the same time, substantial cell death occurs and exhibits regional variation in the dentate gyrus (Gould et al., 1991). Analysis of apoptotic cell death of dentate granule cells by TUNEL assays was performed at postnatal days 0 and 10 in wild-type and L1-minus mice. Increased granule cell death was not observed in L1 mutant mice at any region of the dentate gyrus (rostral, middle, and temporal as defined in Materials and Methods) (Table 3). These results indicate that loss of L1 did not increase granule cell death during the peak period of neurogenesis. In addition, commissural/associational axons of pyramidal cells and afferents from the septum and entorhinal cortex normally synapse with dentate granule cells during the first 2 postnatal weeks (Loy et al., 1977).

Table 2. Number of hippocampal cells is decreased in L1-minus mice

	Wild type ($n = 4$)	L1-minus ($n = 3$)
Pyramidal neurons ($\times 10^5$)	2.6 ± 0.2	1.8 ± 0.1*
Granule neurons ($\times 10^5$)	5.8 ± 0.6	4.3 ± 0.3*
Pyramidal layer glia ($\times 10^5$)	1.6 ± 0.2	1.0 ± 0.1*
Granular layer glia ($\times 10^5$)	0.6 ± 0.1	0.5 ± 0.1
Pyramidal layer (mm^3)	0.78 ± 0.07	0.56 ± 0.03*
Granular layer (mm^3)	0.28 ± 0.03	0.21 ± 0.02*
Mean body weight (gm)	23.3 ± 0.8	26.0 ± 0.6

n, Number of mice. Data are for one hemisphere.

*Significant difference by one-tailed *t* test ($p \leq 0.05$).

Table 3. Density of TUNEL-positive cells in the hippocampus and septum of L1-minus mice

	TUNEL-positive cells (10^6 μm^2)[a]	
	L1-minus	Wild type
Dentate gyrus[b] (PD0)		
Rostral	50 ± 14	51 ± 6
Middle	32 ± 7	30 ± 2
Temporal	22 ± 4	21 ± 7
Dentate gyrus (PD10)		
Rostral	33 ± 7	46 ± 7
Middle	11 ± 3	13 ± 4
Temporal	8 ± 2	8 ± 2
Pyramidal layer (PD0)	43 ± 8	37 ± 5
Pyramidal layer (PD10)	4 ± 1	6 ± 1
Septum (PD0)	15 ± 2	17 ± 3
Septum (PD10)	12 ± 2	10 ± 1

For postnatal day 1 (PD1), data represent three L1-minus and two wild-type mice; for postnatal day 10 (PD10), two L1-minus and two wild-type mice. L1-minus and wild-type means were not significantly different at $p < 0.05$.

[a]Values indicate mean ± SEM.

[b]Defined in Materials and Methods.

Failure of synaptogenesis attributable to the absence of L1 might result in loss of granule cell survival. However, neither hippocampal pyramidal cells nor septal cells of L1-minus mice exhibited increased cell death at postnatal days 0 or 10 (Table 3). Thus the lack of L1 did not seem to cause cell death in these areas during the major period of synaptogenesis. Nonetheless, L1 might contribute to mechanisms of granule cell birth or death at later stages of development because granule cell neurogenesis, synaptogenesis, and cell death extend from the second postnatal week well into adulthood (Gould et al., 1991).

Golgi staining showed that all types of neurons and interneuronal connections found in the wild-type hippocampus were present in the hippocampus of L1-minus mice (Fig. 2*B*). Most granule and pyramidal cells (Fig. 2*B,C*) displayed normal cytoarchitecture; however, near the medial wall of the hippocampus a few pyramidal cells were observed with atypically curved, wavy dendrites (Fig. 2*A*). In addition some granule cells of the dentate gyrus were displaced from their location in the granular layer and had dendrites that were oriented perpendicular to the dendritic arbor of other granule cells (Fig. 2*D,E*). Atypical dendritic morphology and displaced neurons were infrequently seen in L1-minus mice but were never observed in sections from wild-type mice.

Abnormalities in pyramidal cell dendrites in the cerebral cortex

The size and general structure of the cerebral cortex of L1-minus mice were not grossly different from those of wild-type mice. All cortical layers were present. Measurements of cortical size in Nissl-stained sections from equivalent sites showed that the widths of the primary and secondary motor cortex, the somatosensory cortex, and visual cortex of L1 mutant mice did not differ from the wild-type cortical regions (Table 4). In addition, the relative distribution and size classes of neuronal cells in the L1-minus cortex seen by differential contrast microscopy (data not shown) revealed no obvious alteration in cortical lamination; thus, unlike the *reeler* mutation, migration of neuronal precursors on radial glia [which lack L1 (Fushiki and Schachner, 1986)], and their subsequent displacement by later differentiating neurons to form the inside-out lamination of the cortex, did not seem to be perturbed in L1 knockout mice.

Examination of Golgi preparations revealed that the cerebral cortex of L1 mutant mice contained a significant fraction of pyramidal neurons with abnormal dendritic morphologies in motor, visual, and somatosensory areas. In the motor cortex of wild-type mice, typical pyramidal cells displayed well developed apical dendrites that were straight, reached layer I, and had numerous branches that extended horizontally, as in the case of wild-type mice (Fig. 3*A*). Basal dendrites were well formed, with branches of three to four orders. Both apical and basal dendrites were covered with numerous spines. Although L1-minus mice exhibited many typical pyramidal cells in both the primary and secondary motor cortex, a significant fraction of pyramidal neurons failed to display the characteristic upright apical dendrite terminating in layer I (11% of pyramidal neurons in our Golgi-impregnated sections). These pyramidal cells, whose bodies lay primarily in layers II and V of the motor cortex, had laterally directed apical dendrites with respect to layer I (Fig. 3*B,C*).

In the visual cortex of the L1-minus mouse, there were many atypical pyramidal neurons whose bodies lay in layers V–VI (62% of Golgi-impregnated neurons). These atypical pyramidal neurons (Fig. 3*F–J*) differed from normal pyramidal neurons (Fig. 3*E*) in having nonlinear, undulating apical dendrites that were morphologically distinct from the straight apical dendrites of normal pyramidal cells. Pyramidal neurons with undulating apical dendrites were also seen at a high frequency (50% of Golgi-impregnated neurons) in layers V–VI of the somatosensory cortex (Fig. 3*L*) and were clearly different from those in the corresponding region of the wild-type cortex (Fig. 3*K*). In some ways the atypically curved apical dendrites of pyramidal neurons in the cortex of L1 mutant mice resembled immature dendrites seen in Golgi preparations of prenatal and early postnatal rats (Wise et al., 1979). A majority of the apical dendrites of Golgi-stained pyramidal cells of layer V terminated in layer IV (Fig. 3*D*; visual cortex), and only occasionally attained layer I. These dendrites appeared to lack the highly branched apical tufts that form connections with components of layer I. In contrast, many pyramidal cells from layers II and III did display apical tufts (data not shown). Because Golgi impregnation labels only a small proportion of neurons, it was not possible to conclude with certainty that layer V pyramidal cells lacked apical tufts entirely. It is unlikely, however, that the majority of these neurons represented the normal population of callosally projecting pyramidal neurons whose dendrites terminate in layer IV (Koester and O'Leary, 1992, 1994), because apical dendrites of wild-type callosal neurons exhibit an upright morphology.

To compare quantitatively the undulation of normal and mutant apical dendrites, a linearity index was calculated by computer-assisted measurement of apical dendrite lengths of layer V pyramidal neurons in Golgi-stained sections of adult visual cortex. The linearity index (L) was defined as the curvilinear length (in micrometers) of a region of the apical dendrite divided by the linear (radial) distance between the ends of the region of dendrite measured. The mean linearity index ($\pm$SE) for apical dendrites ($n = 52$) of pyramidal neurons from three L1-minus mice was 1.23 ± 0.01, whereas that of apical dendrites ($n = 67$) from three wild-type mice was 1.03 ± 0.002. Means were significantly different when analyzed by the two-tailed t test ($p < 0.001$). Thus the apical dendrites of L1-minus layer V pyramidal neurons deviated significantly in linearity from those of wild-type neurons. These findings suggest that dendritic differentiation depends on a functional L1 molecule during development.

Qualitatively the atypical pyramidal cells in the motor, visual, and somatosensory cortex of the L1 mutant brain showed less branching of the apical dendrite and shorter basal dendrites with fewer branches, but it would be necessary to quantitate these aspects of morphology to ascertain this impression. Neurons in the frontal associative area (Franklin and Paxinos, 1997) of the cortex in the rostral part of the brain were without pathology.

L1 expression is developmentally regulated in the normal mouse brain

Immunocytochemical staining of the brain of fetal (E18) wild-type mice showed that L1 was expressed in regions that were abnormal in the L1 mutant mice (the hippocampus, corpus callosum, and cerebral cortex) (Fig. 4*A*). In addition to the corpus callosum, L1 staining was evident in other fiber tracts, including the internal capsule, fimbria, stria terminalis, and habenulopeduncular tract (Fig. 4*A*). No significant L1 immunoreactivity was seen in ependymal cells lining the lateral ventricles (*LV*) or third ventricle (Fig. 4*E*, *left*) at this or later stages of development. No staining was seen in the E18 brain when nonimmune IgG was used as control (Fig. 4*E*, *left*). In addition, L1 immunoreactivity was not observed in mouse embryos (E9 and E14,

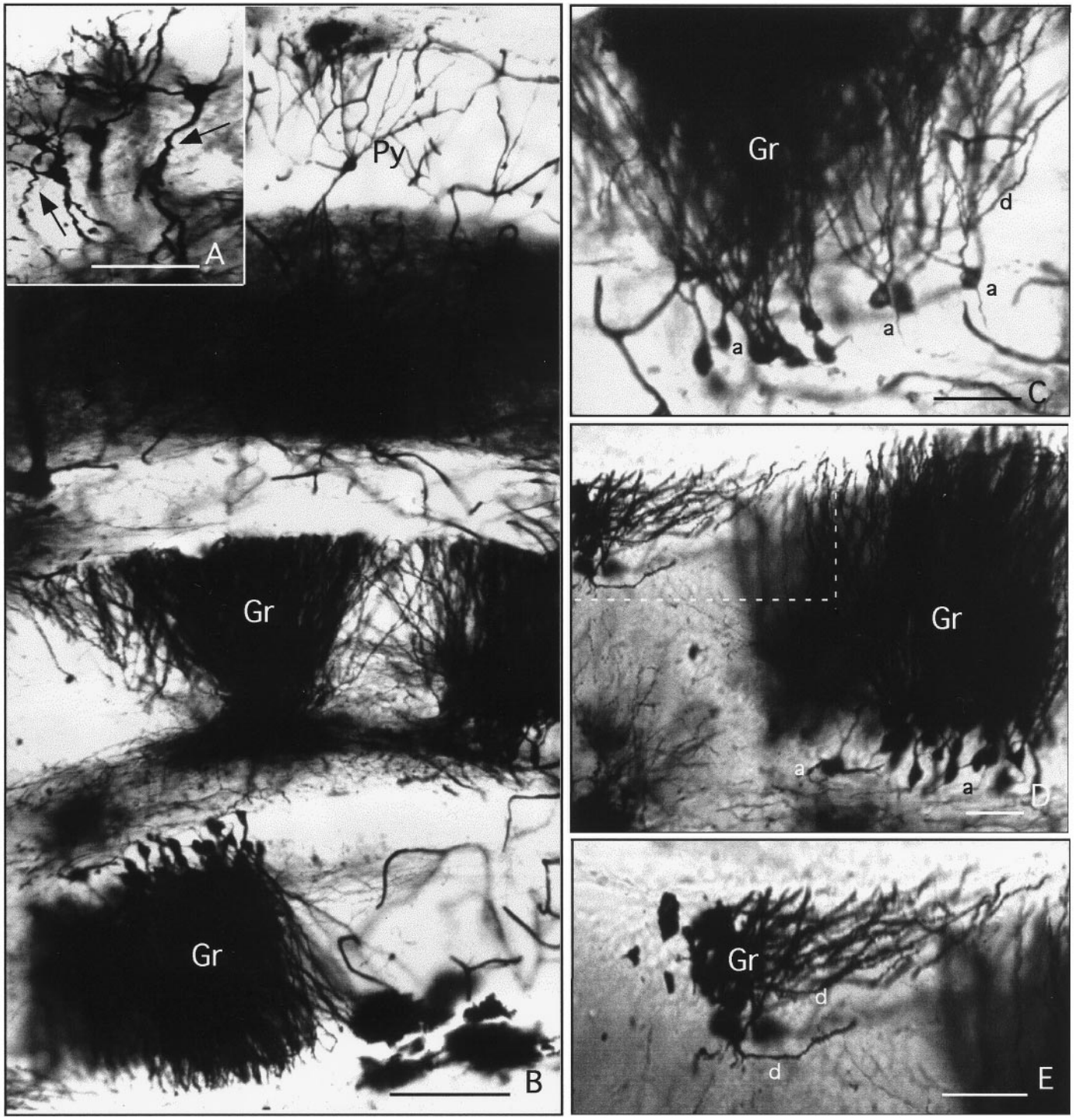

Figure 2. Cytoarchitecture of the smaller L1-minus hippocampus showing pyramidal and granule cell abnormalities. Frontal sections of the L1-minus mouse brain containing the hippocampus were stained by the Golgi technique to reveal neuronal cell bodies and their processes. *Py*, Pyramidal neuron; *Gr*, granule neuron; *a*, axon; *d*, dendrite. *A*, Pyramidal cells with atypical wavy dendrites (*arrows*). Scale bar, 50 μm. *B*, Section showing the CA1 region of the pyramidal layer and the dentate gyrus with normal layers and cytoarchitecture. Scale bar, 100 μm. *C*, Granule cells in dentate gyrus showing axons (*a*) and dendrites (*d*) with a normal orientation. Scale bar, 50 μm. *D*, Region of dentate gyrus with a group of displaced granule cells bearing misoriented dendrites (*box* delineated by *dashed line*). Scale bar, 50 μm. *E*, Higher magnification of area delineated by *dashed line* in *D*. Scale bar, 50 μm.

somite stage) during early stages of neural tube formation (data not shown).

In the hippocampus at E18, L1 immunoreactivity was evident in the developing pyramidal layer [stratum pyramidale (SP)] of wild-type mice (Fig. 4*B*). By postnatal day 33 (*Pd33*), L1 immunoreactivity had decreased in the hippocampus but was moderately intense in approximately one-third of the cell bodies located in the stratum pyramidale and granular layer (*Gr*) of the dentate gyrus (Fig. 4*C*). Lower level L1 staining was present in process-rich regions: the stratum oriens (*SO*), stratum radiatum (*SR*), and

Table 4. Size of cerebral cortex is not altered in L1-minus mice

	Width of cortex (μm ± SE)	
Cortical region	Wild type (n = 5)	L1-minus (n = 2)
Primary motor	1017 ± 55	1052 ± 144
Secondary motor	1051 ± 35	1032 ± 63
Somatosensory	1111 ± 54	1214 ± 108
Visual	759 ± 22	712 ± 73

n, Number of mice.
No significant difference by two-tailed t test ($p > 0.05$).

stratum moleculare (*SM*). No staining was seen in the normal Ig control (Fig. 4*E*, *middle*). In the adult hippocampus (postnatal day 150), moderate L1 immunoreactivity was seen in the stratum lacunosum moleculare (*SL*), with low but persistent levels of L1 staining in the process-rich layers (Fig. 4*D*) compared with control staining (Fig. 4*E*, *right*). The general decline in L1 expression during maturation of the hippocampus was in accord with other reports. Persohn and Schachner (1990) described a decline in L1 expression from embryonic stages with little or no staining of neuronal cell bodies and weak staining of axon-rich layers at postnatal day 21, but adult expression was not examined. Miller et al. (1993) reported a pattern of L1 expression in the adult mouse hippocampus similar to ours, with the stratum lacunosum moleculare showing moderate staining and little staining of the pyramidal cell bodies, mossy fiber tract, or hilus.

L1 was prominently expressed in developing neurons of the neocortex at E18, as shown in the visual cortex (Fig. 4*F*). Strong labeling was evident in the marginal zone and in neuronal cell bodies in the intermediate zone, but less was seen in the cortical plate and ventricular zone, in accord with earlier studies (Fushiki and Schachner, 1986; Beasley and Stallcup, 1987; Chung et al., 1991). L1 expression in the cortex declined with maturation, so that by postnatal day 33 L1 staining was seen primarily in a subset of cell bodies of the developing cortical layers II–V (Fig. 4*G*). In the adult visual cortex, further reduction in L1 expression occurred in cells of layers II–V (Fig. 4*H*). At higher magnification, L1 immunoreactivity could be seen associated with cells within the cortex (Fig. 4*H*, *insert* at *bottom*).

L1 was very evident in the corpus callosum of wild-type mice at E18 (Fig. 4*I*), a stage in which callosal axons in the rodent brain are actively engaged in migration across the midline (Valentino and Jones, 1982; Koester and O'Leary, 1994). L1 staining declined dramatically in the corpus callosum from E18 to postnatal day 33 (Fig. 4*J*) and was not evident in the adult (data not shown). Some reaction product seen in the region of the choroid plexus (Fig. 4*J*) did not appear localized to cellular structures at higher magnification. Downregulation of L1 in the corpus callosum on maturation might serve to prevent further growth of cortical axons across the midline and may be the consequence of myelination, as suggested for the similar decline in L1 during maturation of the optic and sciatic nerves (Martini and Schachner, 1988; Bartsch et al., 1989). The Probst bundles of the L1-minus mouse brain were prominently labeled with antibodies against myelin basic protein in accord with identification as myelinated axons that formed neuromatous bundles (Fig. 4*K*). Probst bundles were also characterized by staining for GFAP. GFAP-positive astrocytes are normally distributed randomly throughout the corpus callosum (LaMantia and Rakic, 1990), and they are present in Probst bundles of acallosal mice (Smith et al., 1986). Medium-sized GFAP-positive cells with a stellate morphology typical of astrocytes were observed throughout the presumptive Probst bundles of the L1-minus mouse brain (Fig. 4*L*). These results suggest that L1 has a normal function in guidance of callosal axons across the midline rather than permissive axon outgrowth. It should be noted that similar results on L1 expression in the hippocampus, cerebral cortex, and corpus callosum were obtained with monoclonal antibodies against L1 (antibody 324; Boehringer Mannheim). In addition, no staining of brain sections from postnatal day 1 or adult L1-minus mice was observed by immunoperoxidase staining with the polyclonal L1 antibody 6096.

L1 is localized preferentially in axons in the mature hippocampus (Persohn and Schachner, 1990) and cerebellum (Persohn and Schachner, 1987), but its subcellular localization in cortical neurons during development is not clear. To examine this in the developing cerebral cortex, we performed double immunofluorescence staining for L1 (fluorescein) and MAP2 (rhodamine), a neuron-specific protein enriched in neuronal dendrites and somata (Matus, 1988), using sections of embryonic day 18 visual cortex. By confocal microscopy, coincident labeling of L1 and MAP2 (yellow color overlay) was observed in the marginal zone and cortical plate (Fig. 4*M*). Figure 4*N* shows differential interference microscopy of the same field. Coincident staining of L1 and MAP2 in the cortical plate appeared to be present in processes oriented perpendicular to the pial surface (*arrows*) and in a number of cell bodies. This suggests that L1 might be localized either in apical dendrites of cortical neurons or in cortical axons in close apposition to or direct contact with apical dendrites. Radial glia have been shown previously to be L1 negative (Fushiki and Schachner, 1986). A small amount of fluorescein staining alone may correspond to L1 in axons, whereas rhodamine staining alone surrounded a smaller proportion of cell bodies. Nonimmune IgG controls were negative (Fig. 4*O*). The polyclonal L1 antibody used (6096) did not produce any immunofluorescence staining of the visual cortex of L1-minus mice monitored by confocal microscopy (data not shown). These results suggest that L1 may be present in apical dendrites of developing cortical neurons in addition to its localization in axons of mature neurons.

DISCUSSION

New findings concerning the phenotype of L1-minus mice reported here are its abnormal dendritic architecture, decreased numbers of hippocampal neurons, and dysgenesis of the corpus callosum. These features suggest new aspects of L1 function in neural development, and together with the previously described dilation of the ventricular system, they underscore the potential for the L1 knockout as a mouse model for human CRASH syndrome.

The presence of undulating apical dendrites of layer V pyramidal neurons in sensory cortical regions of L1 mutant mice suggests a role for L1 in dendritic morphogenesis. Apical dendrites of pyramidal neurons in prenatal development contact elements of the marginal zone, including Cajal-Retzius cells, corticopetal and Martinotti cell axons, and elaborate apical tufts in this region (Marin-Padilla, 1992). Binding between apical dendrites and one or more of these components could be mediated by homophilic or heterophilic L1 binding, because L1 is present on neuronal processes in the marginal zone, is expressed by Cajal-Retzius cells (Fushiki and Schachner, 1986), and might be present on apical dendrites. If critical adhesive interactions between these components do not occur in the L1 mutant, den-

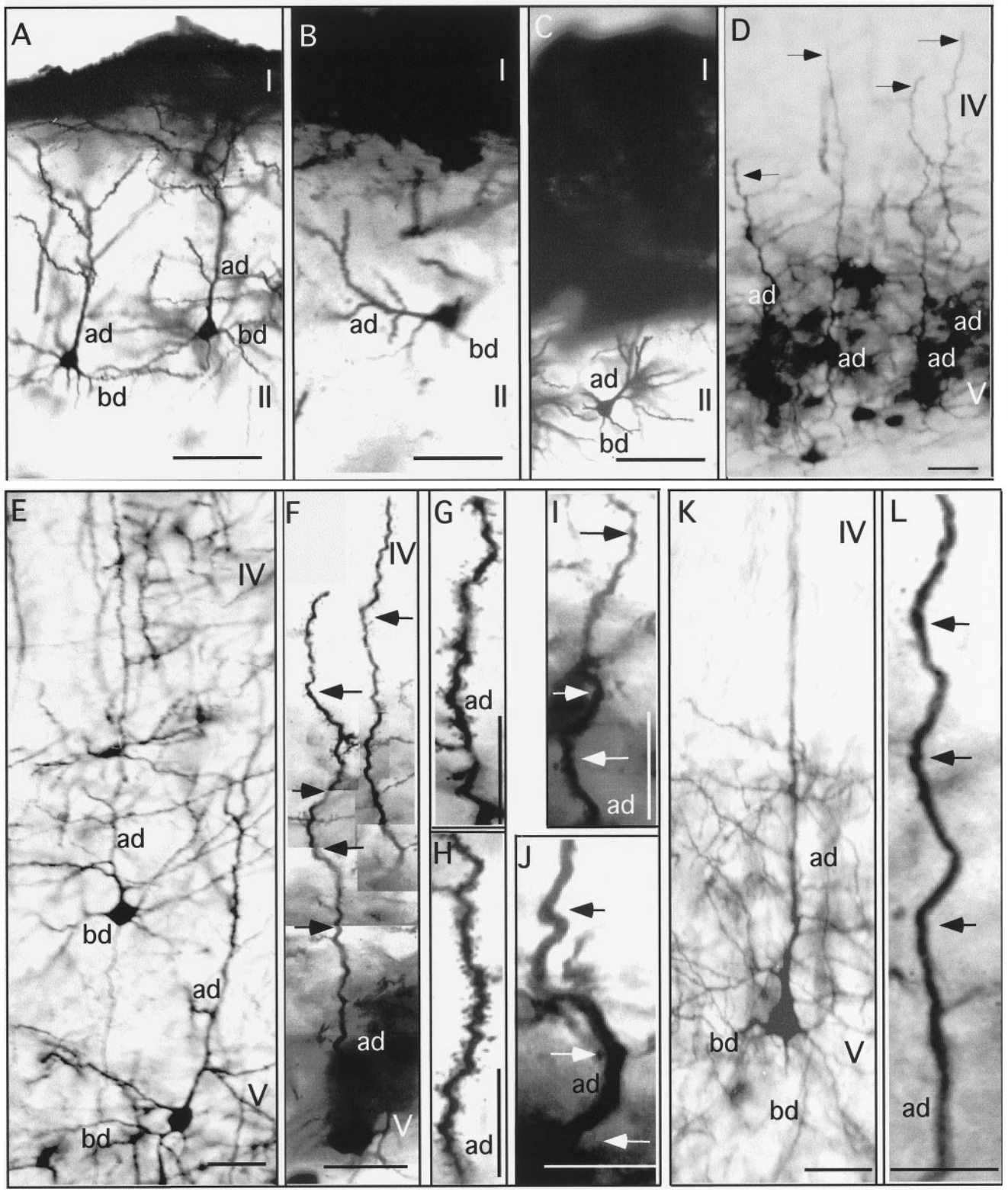

Figure 3. Abnormal apical dendrites of pyramidal neurons in the L1-minus cerebral cortex. Frontal sections through the wild-type and L1-minus brain were stained by the Golgi technique to reveal neuronal cell bodies and their processes in different regions of the cerebral cortex. Scale bars, 50 μm. *A*, Motor cortex of wild-type mouse showing normal pyramidal cell in layer II with well developed apical and basal dendrites. *B, C*, Motor cortex of L1-minus mice showing pyramidal cells in layer II with apical dendrites (*ad*) that were directed laterally with respect to layer I (*I*). *D*, Visual cortex of L1-minus mouse showing layer V pyramidal cells with apical dendrites lacking apical tufts (*arrows*) terminating in layer IV. *E*, Visual cortex of wild-type mouse showing pyramidal neurons in layers V–VI with straight and well formed apical dendrites (*ad*) and basal dendrites (*bd*). *F–J*, Visual cortex of L1-minus mice showing pyramidal neurons in layer V with wavy apical dendrites terminating in layer V (*arrows*) and reduced branching. Computer reconstruction in *F* was used to align focal planes. *K*, Somatosensory cortex of wild-type mouse showing pyramidal neurons in layers V–VI with straight and highly branched apical dendrites. *L*, Somatosensory cortex of L1-minus mouse showing a pyramidal neuron in layers V–VI with a curved apical dendrite (*arrows*).

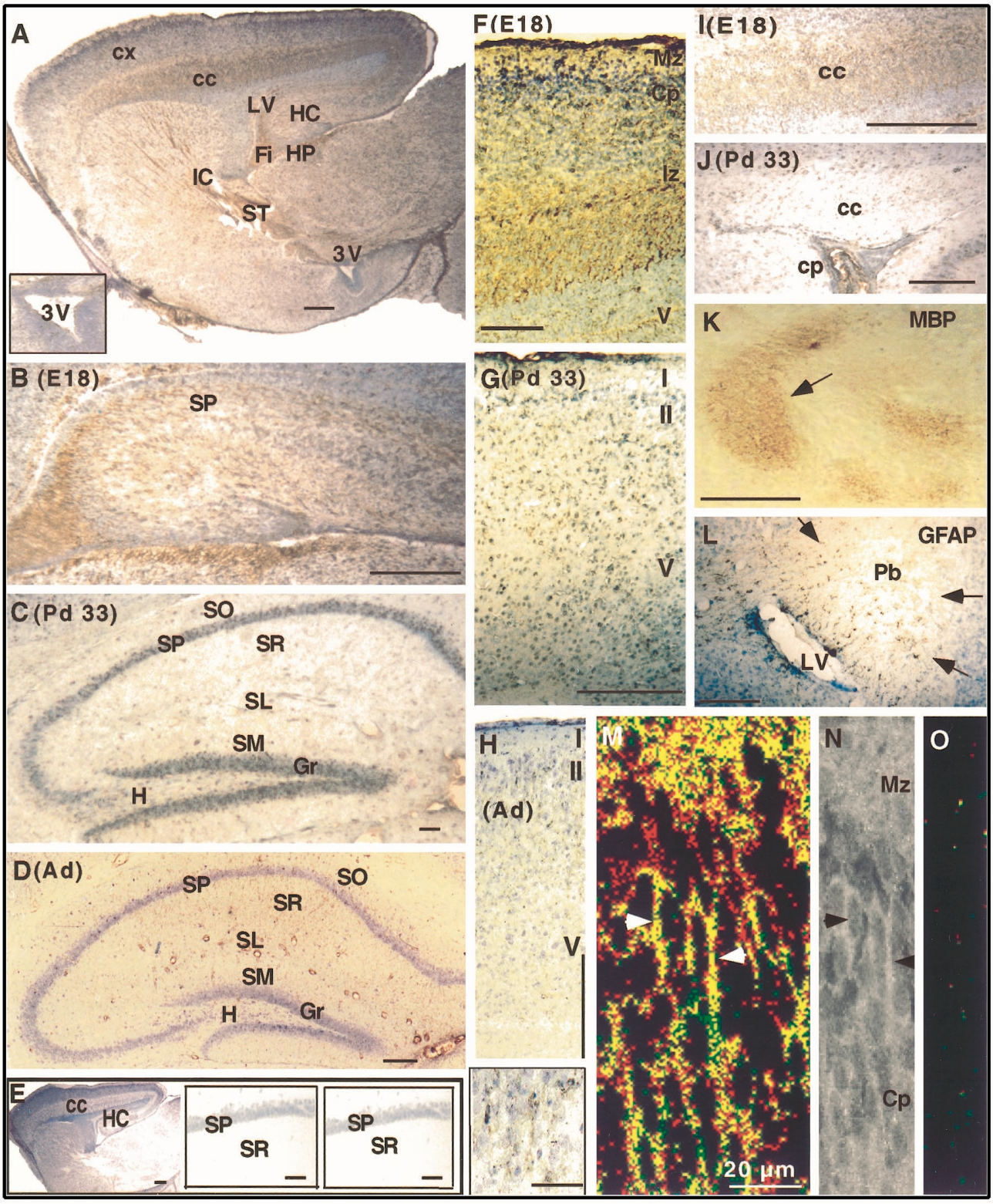

Figure 4. Developmental regulation of L1 expression in wild-type mouse brain. Immunoperoxidase staining of fixed sections of wild-type mouse brain at embryonic day 18 (*E18*), postnatal day 33 (*Pd 33*), and adult stained by the avidin–biotinylated peroxidase method using rabbit polyclonal antibody 6096 directed against L1 and counterstained with toluidine blue. Scale bar, 200 μm. *A*, Sagittal section from E18 mouse brain showing L1 strongly expressed in the cerebral cortex (*cx*), corpus callosum (*cc*), internal capsule (*IC*), stria terminalis (*ST*), hippocampus (*HC*), fimbria (*Fi*), and habenulo-peduncular tract (*HP*). Ependymal cells lining the lateral ventricle (*LV*) and third ventricle (*3V*; *insert* magnification threefold) were not stained. *B*, Hippocampus of E18 brain showing strong L1 staining in the developing stratum pyramidale (*SP*). *C*, Frontal section of postnatal day 33 hippocampus showing moderate L1 staining of approximately one-third of cell bodies in the SP and granular (*Gr*) layers, and low-level L1 staining in the stratum oriens (*S*), stratum radiatum (*SR*), and stratum moleculare (*SM*). *D*, Frontal section of adult (*Ad*) hippocampus showing moderate L1 staining of the stratum lacunosum moleculare (*SL*), low-level staining of process-rich layers, and no staining of the SP or (*Figure legend continues*)

dritic growth cones might lose attachment to layer I, fail to develop apical tufts, and wander, resulting in undulation, because differentiating neurons displace the cell bodies of pyramidal neurons to lower layers during cortical lamination. Such a mechanism is consistent with the demonstrated neurite growth-promoting ability of L1 (Lagenaur and Lemmon, 1987; for review, see Kamiguchi et al., 1998).

Dendritic maturation (but not the vertical orientation and general dendritic tree) is also modulated by neuronal activity (Valverde, 1968; Harris and Woolsey, 1981; Katz and Constantine-Paton, 1988; Katz et al., 1989; Bailey and Kandel, 1993). L1 could contribute indirectly to activity-dependent dendritic differentiation through effects on axon fasciculation or initial target recognition required for synapse formation. Because neurotrophins also stimulate dendritic growth and remodeling (McCallister et al., 1996, 1997), L1 signaling might integrate with the pathways stimulated by neurotrophin receptors of the Trk family as well as with electrical activity to regulate dendritic development coordinately. In support of this notion, L1 signaling activates the MAP kinase cascade culminating in phosphorylation of the transcription factor cAMP-response element binding protein (CREB) (Schmid et al., 1999), a pathway shared by all three Trk receptors (Ginty et al., 1993; Ghosh et al., 1994). These new findings suggest that L1, and possibly other cell adhesion molecules (CAMs) such as neural CAM (NrCAM) and their signaling components, may be critical determinants in the poorly understood mechanism of cortical dendrite differentiation, a hypothesis that can be tested using genetic knockout mice.

The decrease in hippocampal neuronal number in the L1 knockout mouse may result from defects in cell proliferation, migration/synaptogenesis, or survival. L1 has been shown to function as a survival factor for dopaminergic neurons in culture (Hulley et al., 1998). However, the lack of increased death of granule cells in the dentate gyrus of early postnatal L1-minus mice suggests that L1 does not participate in the major period of granule cell neurogenesis, migration, or death (Gould et al., 1991). The major period of synaptogenesis in the dentate gyrus also occurs in the first 2 postnatal weeks (Loy et al., 1977), but because cell death did not increase in granule, pyramidal, or septal cells during this time, it is unlikely that survival mechanisms dependent on synaptogenesis failed at this stage of development. Nonetheless, L1 might contribute to mechanisms of granule cell birth or activity-dependent cell survival at later stages of development, because granule cell neurogenesis and cell death continue at reduced rates from the second postnatal week well into adulthood (Gould et al., 1991). A decrease in hippocampal neurons could be difficult to detect if it occurred throughout the postnatal to adult period.

The regular spacing of radial glia in the secondary proliferative zone of the hilus indicates that glial proliferation may be regulated coordinately with the number of neurons (Rickmann et al., 1987). Coordinate regulation might explain the proportionate decrease in glia in the L1-minus hippocampus. The reduced number of hippocampal neurons could contribute to the spatial learning deficits of L1 mutant mice (Fransen et al., 1998). Although most studies support a view that LTP in the hippocampal CA1 region underlies spatial learning (Chen and Tonegawa, 1997), we did not detect alterations in LTP at the CA1 synapse in hippocampal slice preparations from L1-minus mice (J. Kauer and P. F. Maness, unpublished observations).

Two mechanisms could explain the impaired ability of callosal axons to cross the midline in the L1 mutant brain. L1, which is present on migratory callosal axons, may act as a cue to direct growth cones to cross the midline, analogous to its ability to stimulate the growth of neurites in culture (Ignelzi et al., 1994). Growth cones of callosal axons bear a complex morphology typical of those at choice points because they interdigitate among opposing axons and astroglia without forming specialized contacts or fasciculating in a topographic order (Norris and Kalil, 1990). Midline pathfinding errors attributable to loss of L1 have been shown for the decussation of axons in the corticospinal tract of L1-minus mice (Cohen et al., 1997), and closely related Nr-CAM is needed for commissural axon trajectory across the chick spinal cord floorplate (Stoekli and Landmesser, 1995). However, in caudal regions of the corpus callosum, L1-related defects in the closing of the longitudinal fissure may create a physical barrier to axon crossing. Certain "acallosal" substrains of inbred mice, including 129/J and 129/ReJ, display partial or complete absence of the corpus callosum (Lipp and Wahlsten, 1992; Livy and Wahlsten, 1997), the frequency of which can be influenced by maternal environment and rearing conditions (Wahlsten, 1982). Defects in these mice are multigenic (Wahlsten, 1989) and have been attributed to delayed formation of the hippocampal commissure and abnormal closure of the longitudinal fissure (Valentino and Jones, 1982). In some strains, retarded growth of the septum contributes to the abnormality, but this is not a defect found in the 129 strain of mice (Wahlsten and Bulman-Fleming, 1994). In contrast, the 129/SvJae substrain used in our studies always displayed an intact corpus callosum of normal size without Probst bundles and a well formed septum; thus the defects observed in the L1 knockout mice appeared to be specific consequences of the loss of L1. However, these studies illustrate that abnormalities of the longitudinal fissure and septum can contribute to callosal agenesis.

The enlarged ventricular system in the L1 knockout mice studied here was in agreement with a magnetic resonance imaging study of L1 null mice (Fransen et al., 1998). Both studies showed ventricular enlargement; however, enlargement of only the lateral and fourth ventricles (but not the third ventricle) and an altered shape but not size of the aqueduct were reported in the

←

Gr layers. *E*, Normal Ig control staining of E18 mouse brain (*left*), Pd33 hippocampus (*middle*), and adult hippocampus (*right*). *F*, Frontal section of the E18 visual cortex showing L1 staining in the marginal zone (*Mz*) and intermediate zone (*Iz*), and lower levels of staining in the cortical plate (*Cp*) and ventricular zone (*V*). *G*, Frontal section of Pd 33 visual cortex showing L1 staining of neuronal cell bodies in layers II–V and in processes of layer I. *H*, Frontal section of adult (*Ad*) visual cortex showing reduction of L1 staining in cortical layers I–V. *Insert* (*bottom* of *H*) shows higher magnification of layer II. *I*, Frontal section of E18 showing L1 staining of the corpus callosum. *J*, Frontal section of Pd 33 brain reduction in L1 staining in the corpus callosum. *cp*, Choroid plexus. *K*, Frontal section of adult L1-minus brain showing myelin basic protein (*MBP*) staining of Probst bundle (*arrow*). *L*, Glial fibrillary acid protein immunoreactivity of Probst bundle (*arrows*) adjacent to lateral ventricle (*LV*) of an L1-minus adult mouse. *M*, Frontal section of E18 visual cortex showing double-immunofluorescence staining of L1 (fluorescein) and MAP2 (rhodamine) by confocal microscopy in a computer-generated color overlay. *Yellow* indicates colocalization of L1 and MAP2. *N*, The same field as in *M* visualized by differential interference contrast microscopy. *Black arrows* point to the same sites as *white arrows* in *M*. *O*, Control staining of E18 visual cortex with normal rabbit Ig (fluorescein) and normal mouse Ig (rhodamine) visualized by confocal microscopy in a computer-generated color overlay.

Fransen et al. (1998) study. These minor differences could be attributable to genetic variation in the substrains and/or conditions of rearing (Wahlsten, 1982). Influence of genetic modifiers on ventricular dilation in L1 mutant mice was demonstrated previously by Dahme et al. (1997), who reported enlarged lateral ventricles in L1 mutant mice on C57/Bl6J but not 129/SvEv backgrounds. The enlarged ventricles of L1-minus mice might result from defective neuronal process extension or cell loss in specific regions of the brain. Ventricular dilation was probably not caused by defective adhesion of ependymal cells, because L1 was not detected in these cells by immunocytochemistry.

Many of the phenotypic features of the L1-minus mice mirrored aspects of the human CRASH syndrome. The atypical dendrites of cortical pyramidal cells and decreased number of hippocampal neurons in the L1-minus mouse brain may be relevant to mental retardation and/or motor dysfunction in affected patients. Agenesis/dysgenesis of the corpus callosum, which occurs to varying degrees in humans and L1-minus mice, is known to result in poor performance on tasks involving sensorimotor integration (Lipp and Wahlsten, 1992). The extent of ventricular dilation in L1-minus mice corresponded to the milder forms of hydrocephalus in some CRASH patients but not to the dramatic enlargement of ventricles with high-pressure cerebrospinal fluid in severe cases (Schrander-Stumpel et al., 1995). The L1-minus phenotype also resembled the neuropathological condition of human fetal alcohol syndrome, which includes mental retardation, callosal agenesis, and hydrocephalus (Abel and Sokol, 1987). In rodents, acute ethanol exposure during gestation leads to wide septal nuclei and other midline abnormalities (Sulik et al., 1986), as well as a decrease in hippocampal pyramidal cells (Barnes and Walker, 1981; West and Goodlett, 1990). Interestingly, ethanol exposure of neuroblastoma cells in culture disrupts cell–cell adhesion caused by L1 but not other cell adhesion molecules (Ramanathan et al., 1996). Thus the L1 knockout model may also help in understanding the developmental defects in children of alcoholic mothers.

REFERENCES

Abel EL, Sokol RJ (1987) Incidence of fetal alcohol syndrome and economic impact of FAS-related anomalies. Drug Alcohol Depend 19:51–70.

Atashi JR, Klinz SG, Ingraham CA, Matten WT, Schachner M, Maness PF (1992) Neural cell adhesion molecules modulate tyrosine phosphorylation of tubulin in nerve growth cone membranes. Neuron 8:831–842.

Bailey CH, Kandel ER (1993) Structural changes accompanying memory storage. Annu Rev Physiol 55:397–426.

Barnes DE, Walker DW (1981) Prenatal ethanol exposure permanently reduces the number of pyramidal neurons in rat hippocampus. Dev Brain Res 1:333–340.

Bartsch U, Kirchhoff F, Schachner M (1989) Immunohistological localization of the adhesion molecules L1, N-CAM, and MAG in the developing and adult optic nerve of mice. J Cell Neurosci 284:451–462.

Beasley L, Stallcup WB (1987) The nerve growth factor-inducible large external glycoprotein and neural cell adhesion molecule (NCAM) have distinct patterns of expression in the developing rat CNS. J Neurosci 7:708–715.

Braitenberg V, Schüz A (1983) Some anatomical comments on the hippocampus. In: Neurobiology of the hippocampus (Seifert W, ed), pp 21–37. New York: Academic.

Chen C, Tonegawa S (1997) Molecular genetic analysis of synaptic plasticity, activity-dependent neural development, learning, and memory in the mammalian brain. Annu Rev Neurosci 20:157–184.

Chung WW, Lagenaur CF, Yan Y, Lund JS (1991) Developmental expression of neural cell adhesion molecules in the mouse neocortex and olfactory bulb. J Comp Neurol 314:290–305.

Cohen NR, Taylor JSH, Scott LB, Guillery RW, Soriano P, Furley AJW (1997) Errors in corticospinal axon guidance in mice lacking the neural cell adhesion molecule L1. Curr Biol 7:26–33.

Dahme M, Bartsch U, Martini R, Anliker B, Schachner M, Mantei N (1997) Disruption of the mouse L1 gene leads to malformations of the nervous system. Nat Genet 17:346–349.

Franklin KBJ, Paxinos G (1997) The mouse brain in stereotaxic coordinates. New York: Academic.

Fransen E, Van Camp G, Vits L, Willems P (1997) L1 associated diseases: clinical geneticists divide, molecular geneticists unite. Hum Mol Genet 6:1625–1632.

Fransen E, DíHooge R, Camp GV, Verhoye M, Sijbers J, Reyniers E, Soriano P, Kamiguchi H, Willemsen R, Koekkoek SKE, De Zeeuw CI, De Deyn PP, Van der Linden A, Lemmon V, Kooy RF, Willems PJ (1998) L1 knockout mice show dilated ventricles, vermis hypoplasia and impaired exploration patterns. Hum Mol Genet 7:999–1009.

Freund TF, Antal M (1988) GABA-containing neurons in the septum control inhibitory interneurons in the hippocampus. Nature 336:170–173.

Fushiki S, Schachner M (1986) Immunocytological localization of cell adhesion molecules L1 and NCAM and the shared carbohydrate epitope L2 during development of the mouse neocortex. Dev Brain Res 24:153–167.

Ghosh A, Camahan J, Greenberg ME (1994) Requirement for BDNF in activity-dependent survival of cortical neurons. Science 263:1618–1623.

Ginty DD, Komhauser JM, Thompson MA, Bading H, Mayo KE, Takahash JS, Greenberg ME (1993) Regulation of CREB phosphorylation in the suprachiasmatic nucleus by light and a circadian clock. Science 260:238–241.

Gould E, Woolley CS, McEwen BS, (1991) Naturally occurring cell death in the developing dentate gyrus of the rat. J Comp Neurol 304:408–418.

Harris RM, Woolsey TA (1981) Dendritic plasticity in mouse barrel cortex following postnatal vibrissa follicle damage. J Comp Neurol 196:357–376.

Hulley P, Schachner M, Lubbert H (1998) L1 neural cell adhesion molecule is a survival factor for fetal dopaminergic neurons. J Neurosci Res 53:129–134.

Ignelzi Jr MA, Miller DR, Soriano P, Maness PF (1994) Impaired neurite outgrowth of *src*-minus cerebellar neurons on the cell adhesion molecule L1. Neuron 12:873–884.

Kamiguchi H, Hlavin ML, Yamasaki M, Lemmon V (1998) Adhesion molecules and inherited diseases of the human nervous system. Annu Rev Neurosci 21:97–125.

Katz LC, Constantine-Paton M (1988) Relationships between segregated afferents and postsynaptic neurons in the optic tectum of three-eyed frogs. J Neurosci 8:3160–3180.

Katz LC, Gilbert CD, Wiesel TN (1989) Local circuits and ocular dominance columns in monkey striate cortex. J Neurosci 9:1389–1399.

Klinz SG, Schachner M, Maness PF (1995) L1 and N-CAM antibodies trigger protein phosphatase activity in growth cone-enriched membranes. J Neurochem 65:84–95.

Koester SE, O'Leary DDM (1992) Functional classes of cortical projection neurons develop dendritic distinctions by class-specific sculpting of an early common pattern. J Neurosci 12:1382–1393.

Koester SE, O'Leary DDM (1994) Axons of early generated neurons in cingulate cortex pioneer the corpus callosum. J Neurosci 14:6608–6620.

Lagenaur C, Lemmon V (1987) An L1-like molecule, the 8D9 antigen, is a potent substrate for neurite extension. Proc Natl Acad Sci USA 84:7753–7757.

LaMantia A-S, Rakic P (1990) Cytological and quantitative characteristics of four cerebral commissures in the Rhesus monkey. J Comp Neurol 291:520–537.

Lipp HP, Wahlsten D (1992) Absence of the corpus callosum. In: Genetically defined animal models of neurobehavioural dysfunctions (Driscoll P, ed), pp 217–252. Boston: Birkhauser.

Livy DJ, Wahlsten D (1997) Retarded formation of the hippocampal commissure in embryos from mouse strains lacking a corpus callosum. Hippocampus 7:2–14.

Loy R, Lynch G, Cotman CW (1977) Development of afferent lamination in the fascia dentata of the rat. Brain Res 121:229–243.

Lüthi A, Laurent JP, Figurov A, Muller D (1994) Hippocampal long-term potentiation and neural cell adhesion molecules L1 and NCAM. Nature 373:777–779.

Marin-Padilla M (1987) The Golgi method. In: Encyclopedia of neuro-

science, Vol 1 (Adelman G, ed), pp 470–471. Cambridge, MA: Birkhauser.
Marin-Padilla M (1992) Ontogenesis of the pyramidal cell of the mammalian neocortex and developmental cytoarchitectonics: a unifying theory. J Comp Neurol 321:223–240.
Martini R, Schachner M (1988) Immunoelectron microscopic localization of neural cell adhesion molecules (L1, N-CAM, and myelin-associated glycoprotein) in regenerating adult mouse sciatic nerve. J Cell Biol 106:1734–1746.
Matus A (1988) Microtubule-associated proteins: their potential role in determining neuronal morphology. Annu Rev Neurosci 11:29–44.
McAllister AK, Katz LC, Lo DC (1996) Neurotrophin regulation of cortical dendritic growth requires activity. Neuron 17:1057–1064.
McAllister AK, Katz LC, Lo DC (1997) Opposing roles for endogenous BDNF and NT-3 in regulating cortical dendritic growth. Neuron 18:767–778.
Miller PD, Chung WW, Lagenaur CF, DeKoskey ST (1993) Regional distribution of neural cell adhesion molecule (NCAM) and L1 in human and rodent hippocampus. J Comp Neurol 327:341–349.
Morse WR, Whitesides III JG, LaMantia A-S, Maness PF (1998) $p59^{fyn}$ and $pp60^{c\text{-}src}$ modulate axonal guidance in the developing mouse olfactory pathway. J Neurobiol 36:53–63.
Mosko S, Lynch G, Cotman CW (1973) The distribution of septal projections to the hippocampus of the rat. J Comp Neurol 152:163–174.
Norris CR, Kalil K (1990) Morphology and cellular interactions of growth cones in the developing corpus callosum. J Comp Neurol 293:268–281.
Norris CR, Kalil K (1991) Guidance of callosal axons by radial glia in the developing cerebral cortex. J Neurosci 11:3481–3492.
Paxinos G, Watson C (1986) The rat brain in stereotaxic coordinates, Ed 2. Sydney: Academic.
Persohn E, Schachner M (1987) Immunoelectron microscopic localization of the neural cell adhesion molecules L1 and NCAM during postnatal development of the mouse cerebellum. J Cell Biol 105:569–576.
Persohn E, Schachner M (1990) Immunohistological localization of the neural adhesion molecules L1 and NCAM in the developing hippocampus of the mouse. J Neurocytol 19:807–819.
Ramanathan R, Wilkemeyer MF, Mittal B, Perides G, Charness ME (1996) Alcohol inhibits cell–cell adhesion mediated by human L1. J Cell Biol 133:381–390.
Rickmann M, Amaral DG, Cowan WM (1987) Organization of radial glial cells during the development of the rat dentate gyrus. J Comp Neurol 264:449–479.
Saffell JL, Williams EJ, Mason IJ, Walsh FS, Doherty P (1997) Expression of a dominant negative FGF receptor inhibits axonal growth and FGF receptor phosphorylation stimulated by CAMs. Neuron 18:231–242.
Schachner M (1991) Neural recognition molecules and their influence on cellular functions. In: The nerve growth cone (Letourneau PC, Kater SB, Macagno ER, eds), pp 237–254. New York: Raven.
Schmid R-S, Graff RD, Schaller MD, Chen S, Schachner M, Hemperly JJ, Maness PF (1999) NCAM stimulates the Ras-MAPK pathway and CREB phosphorylation in neuronal cells. J Neurobiol 38:542–555.
Scholey AB, Rose SP, Samani MR, Bock E, Schachner M (1993) A role for the neutral cell adhesion molecule in a late, consolidating phase of glycoprotein synthesis six hours following passive avoidance training of the young chick. Neuroscience 55:499–509.
Schrander-Stumpel C, Höweler C, Jones M, Sommer A, Stevens C, Tinschert S, Israel J, Fryns JP (1995) Spectrum of X-linked hydrocephalus (HSAS), MASA syndrome, and complicated spastic paraplegia (SPG1): clinical review with six additional families. Am J Med Genet 57:107–116.
Simpson E, Linder C, Sargent E, Davisson M, Mobraaten L, Sharp J (1997) Genetic variation among 129 substrains and its importance for targeted mutagenesis in mice. Nat Genet 16:19–27.
Smith GM, Miller RH, Silver J (1986) Changing role of forebrain astrocytes during development, regeneration failure, and induced regeneration upon transplantation. J Comp Neurol 251:23–43.
Sorge LK, Levy BT, Maness PF (1984) $pp60^{c\text{-}src}$ is developmentally regulated in the neural retina. Cell 36:249–257.
Stoeckli ET, Landmesser LT (1995) Axonin-1, Nr-CAM, and Ng-CAM play different roles in the *in vivo* guidance of chick commissural neurons. Neuron 14:1165–1179.
Sulik KK, Johnston MC, Daft PA, Russell WE, Dehart DB (1986) Fetal alcohol syndrome and DiGeorge anomaly: critical ethanol exposure periods for craniofacial malformations as illustrated in an animal model. Am J Med Genet [Suppl] 2:97–112.
Valentino KL, Jones EG (1982) The early formation of the corpus callosum: a light and electron microscopic study in foetal and neonatal rats. J Neurocytol 11:583–609.
Valverde F (1968) Structural changes in the area striata of the mouse after enucleation. Exp Brain Res 5:274–292.
Wahlsten D (1982) Deficiency of corpus callosum varies with strain and supplier of mice. Brain Res 239:329–347.
Wahlsten D (1989) Genetic and developmental defects of the mouse corpus callosum. Experientia 45:828–838.
Wahlsten D, Bulman-Fleming B (1994) Retarded growth of the medial septum: a major gene effect in a callosal mice. Dev Brain Res 77:203–214.
West JR, Goodlett CR (1990) Teratogenic effects of alcohol on brain development. Ann Med 22:319–325.
West MJ, Andersen AH (1980) An allometric study of the area dentata in the rat and mouse. Brain Res Rev 2:317–348.
Wise SP, Fleshman Jr JW, Jones EG (1979) Maturation of pyramidal cell form in relation to developing afferent and efferent connections of rat somatic sensory cortex. Neuroscience 4:1275–1297.
Wong EV, Kenwrick S, Willems P, Lemmon V (1995) Mutations in the cell adhesion molecule L1 cause mental retardation. Trends Neurosci 18:168–172.
Yamasaki M, Thompson P, Lemmon V (1997) CRASH syndrome: mutations in the L1 gene correlate with severity of the disease. Neuropediatrics 28:175–178.